LA-UR-20-29986 (Accepted Manuscript)

Insight into the chemistry of TNT during shock compression through ultrafast absorption spectroscopies

Powell, Michael Stephan
Moore, David Steven
Mcgrane, Shawn David

To be published in: The Journal of Chemical Physics

DOI to publisher's version: 10.1063/5.0032018

Permalink to record: http://permalink.lanl.gov/object/view?what=info:lanl-repo/lareport/LA-UR-20-29986

Insight into The Chemistry of TNT During Shock Compression Through Ultrafast Absorption Spectroscopies

M. S. Powell[1*], D. S. Moore[2], and S. D. McGrane[2]

[1]High Explosives Science and Technology Group, Los Alamos National Laboratory, Los Alamos, NM 87545, USA
[2]Shock and Detonation Physics Group, Los Alamos National Laboratory, Los Alamos, NM 87545, USA
*-Corresponding Author, email: mspowell@lanl.gov

Abstract: Thin films of trinitrotoluene (TNT) were shock compressed using the ultrafast laser shock apparatus at Los Alamos National Laboratory. Visible (VIS) and mid-infrared (MIR) transient absorption spectroscopies were simultaneously performed to probe for electronic and vibrational changes during shock compression of TNT. Three shock pressures (16, 33, 45 GPa) were selected to observe no reaction, incipient reaction, and strongly developed reactions for TNT within the experimental time scale of <250 ps. Negligible absorption changes in MIR or VIS absorptions were observed at 16 GPa. At 33 GPa, MIR absorptions in the 3,000-4,000 cm^{-1} range were observed to increase during the shock and continue to increase during the rarefaction, in contrast to the VIS absorption measurements, which increased during the shock and almost fully recovered during rarefaction. At 45 GPa both VIS and MIR absorptions were strong and irreversible. The intense and spectrally broad MIR absorptions were attributed to short lived intermediates with strong, spectrally broad absorptions that dominate the spectral response. The MIR and VIS absorption changes observed at 33 and 45 GPa were credited to shock induced chemistry, most likely including formation of a very broad hydrogenic stretch feature. Results from these experiments are consistent with the chemical mechanisms that include O-H or N-H formation such as CH_3 oxidation or C-N homolysis.

I. Introduction

Trinitrotoluene (TNT) is a relatively insensitive high explosive (HE), compared to most secondary HE, that was developed in the late 1800's. Uses of TNT range from defense applications to underwater mining operations. The usage of TNT is currently being phased out due to environmental contamination and health hazards associated with TNT, but the process has been slow due to several favorable traits that TNT

possesses. Due to the large disparity between its melting and decomposition temperature,[1] TNT is one of the few HE capable of being melt casted into cavities. Melt casting is also very useful when TNT is mixed with higher performing HE like RDX. The detonation velocity and pressure of TNT are adequate for many applications, especially considering the decreased sensitivity to initiation of TNT when compared to other higher performing HE.[1-2] The decomposition chemistry of TNT based on various input conditions and initiation mechanisms has been subject of debate[3-21] particularly its detonation chemistry.[4-5, 9, 14, 22-31]

Emulation of the detonation state can be achieved using shock waves.[32] Multiple decomposition and detonation chemistry mechanisms have been suggested between simulations[11, 22, 25-27, 30-31, 33] and experiments.[4-7, 9-10, 13-21, 23-24] Focusing on the detonation or shock compression paths for experiments, homolysis of the C-N bonds at the nitro group in TNT has been a commonly proposed path.[4-5, 14] Oxidation of the methyl ($-CH_3$) group has been another suggested path for TNT decomposition.[4-5] Bimolecular species of TNT could be formed through Diels-Alder reactions prior to formation of simpler species.[23] Cyclization via the methyl and nitro group,[5] nitrite rotation,[5] or C-H α attack[5, 24] mechanisms have been other possible explanations of TNT detonation chemistry. Models have proposed similar mechanisms for TNT detonation with homolysis of the C-N bonds at the nitro group,[22, 26-27, 29, 31] oxidation of the methyl ($-CH_3$) group, [28] bimolecular reactions,[25, 30] or C-H α attack[22, 28] mechanisms. These intermediates all are mechanisms of the first reactions, which then can branch through several other chemical steps on the way to products.

The goal of this work is to measure the bond specific shock induced chemistry of TNT to gain insight into the first chemical steps that occur during TNT detonation. Measurements of the bond specific chemistry were achieved using the benchtop ultrafast laser driven shock platform at Los Alamos National Laboratory. The apparatus is capable of generating and characterizing shock waves in materials, while simultaneously probing electronic and vibrational absorption spectroscopic changes.[34] Changes observed in the vibrational and visible absorption spectra of shock-compressed TNT will be presented with comparisons to those expected for possible chemical mechanisms. Similar to the previous manuscript on shock compressed

PETN, these results can be used to constrain chemical kinetics and reaction models to aid in the development of higher performing HE.[35]

II. Experimental Methods

The laser driven shock apparatus described in previous publications[34-39] was used for these spectroscopic measurements on shock compressed TNT. The shock drive, interferometry, and spectroscopy beams were simultaneously generated from a single pulse out of a Ti:sapphire chirped pulse amplifier (CPA). Fig. 1 shows a diagram of the beams and geometries used in these experiments. A portion of the 150 ps duration chirped pulse (~6 mJ out of 12 mJ) was used to both generate the shock in a material as well as characterize the wave mechanics through interferometry. A flat top beam was used to generate a ~120 µm diameter shock in the sample. Ultrafast dynamic ellipsometry (UDE) was used to measure the free surface velocity of the aluminum drive layer. Impedance matching to a measurement of the aluminum drive layer free surface velocity was used to determine TNT shock pressures for these experiments. The remaining ~6 mJ beam was compressed in the CPA to 35 fs and was used to generate the broadband visible (VIS) and mid-infrared (MIR) absorption spectroscopy probes. The generated VIS radiation from 450-700 nm was utilized for transient VIS absorption. Two MIR ranges could be generated depending on the compression of the CPA: 1,150-3,000 cm^{-1} or 1,450-4,000 cm^{-1}. The spectral resolution in the lower MIR frequency range was approximately 50 cm^{-1}, while that in the higher MIR frequency range was about 90 cm^{-1}. The former range was useful for viewing the symmetric and antisymmetric nitro stretches (ν_s-NO_2 and ν_a-NO_2 respectively) and a portion of the TNT hydrogenic stretches[40] as well as atmospheric CO_2, while the latter range was useful for viewing all portions of the CH-, NH-, and OH- hydrogenic-stretch region (2,800-3,000, 3,000-3,200, 3,200-3,500 cm^{-1} respectively) for CHNO containing species.[41] The VIS and MIR were simultaneously collected during the experiments; however, the interferometric data were collected from the same substrate without TNT film present immediately prior to spectroscopic measurements. VIS and MIR were collected at 25 ps time steps from -50 ps to 250 ps relative to shock entry into the TNT layer. Temporally this range coincided with spectroscopic measurements collected prior

to the shock, during the shock, and during rarefaction in TNT. Per time step, 25 shots were averaged to give an average spectroscopic response per delay. The 25-shot averaged response for all time delays was defined as an experiment. This experiment was performed four times per substrate and was averaged to give an average response per pressure range. Three pressure ranges were selected for this experiment 16-17, 30-34, and 38-49 GPa which corresponded to unreactive, partial reaction, and reactive chemistry regimes, respectively. The average pressures induced in the sample were reported for the unreactive (16 GPa), partial reactive (33 GPa), and reactive (45 GPa) chemistry regimes.

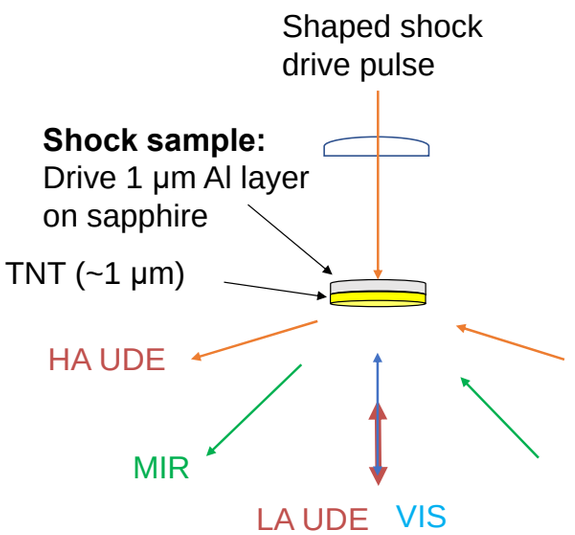

Fig. 1. Diagram of the sample location. High angle UDE was not used for these experiments. Low angle ultrafast dynamic ellipsometry (UDE) was used for impedance matching. Reproduced with permission from J. Phys. Chem. 124, 35 (2020). Copyright 2020 American Chemical Society.[35]

Samples were similar to previous thin film crystal experiments.[34-35, 42] Layers consisted of a tamper material of 500 μm of sapphire, with 1 μm of aluminum vapor deposited onto the tamper, and 1 μm of TNT deposited onto the aluminum drive layer. The thicknesses of aluminum and TNT were chosen to be commensurate with the shock duration of the experiment. TNT was recrystallized in solution to remove potential contaminants from the manufacturing process. The recrystallized TNT was then dissolved in acetone to 16% by mass. This solution was spin cast onto 25.4 mm diameter substrates using 250 μL of solution. Spin casting speed, acceleration, and spin duration parameters were 1500 rpm, 500 rpm/s, and 25

seconds, respectively. Resulting films of TNT were nominally 1 μm in thickness (typically in the range 0.8-1.2 μm). Film thicknesses were measured using a white light interferometer prior to experiments. Typically, the 120 μm diameter shock encompassed between 5-20 TNT crystals. The number of crystals contained in a shock was estimated from both Fig. 2, as well as the density analysis in the supplemental information. Prior to experiments, a portion of the TNT was removed from the substrate. The resulting bare aluminum layer was used for free surface velocity measurements used in impedance matching to the unreactive Hugoniot of TNT. Shown in Fig. 2 is an image of the TNT microstructure. TNT can stabilize into the monoclinic phase with twinning when formed from solutions of acetone.[43-46] Microscopy was performed on multiple TNT substrates prior to experiments. The microstructure observed was similar between substrates. An area analysis was performed on a microscope image to estimate the void fraction and density and is presented in the supplemental material. The void or interfacial scattering regions between crystals were up to 4.65% of the total area as estimated from automated binary analysis of microscopy images of the samples.

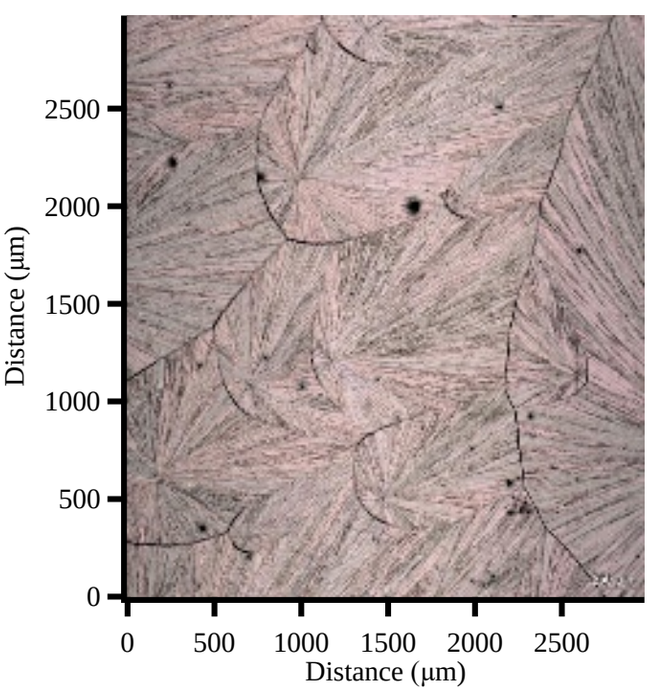

Fig. 2. Image of TNT using white light confocal microscopy. Microstructure was consistent between substrates.

III. Results

1. *Determination of the shock state*

Impedance matching provided a rapid method for determining the pressure induced in the sample by matching the release isentrope of the aluminum drive layer to a linearly extrapolated fit to the unreactive Hugoniot for cream cast TNT.[2] Cream cast TNT was selected for impedance matching due to its high density compared to pressed powders.[2] Three pressure regions labeled low, medium, and high were measured for TNT and are shown in Fig. 3. Low pressure corresponded to pressures that ranged 16-17 GPa, medium pressures were 30-34 GPa, and high pressure were 38-49 GPa. Films 1, 2, and 6 were films that were probed when the MIR frequency was in the 1,150-3,000 cm^{-1} range, while Films 4, 5, 7, and 8 were probed with the 1,450-4,000 cm^{-1} MIR range. In the event that there is a reactive Hugoniot measured in the future, Table S.1 in supplemental information has the free surface velocity of the aluminum drive layer, impedance matched shock and particle velocities for TNT, and the tabulated pressure induced in the sample. Measured free surface velocities were at most 4% different from the average free surface velocity for each pressure range.

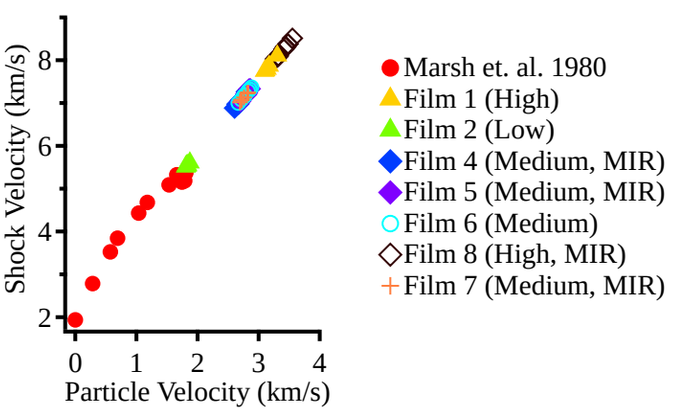

Fig. 3. State determination for shock compressed TNT measured in this experiment. Films labelled MIR were probed with the 1,450-4,000 cm^{-1} MIR range.

2. *Visible (VIS) transient absorption spectroscopy*

The shock transited the film in approximately 180 ps to 120 ps for the low to high pressure range, respectively. Rarefaction of the sample occurred when the shock has fully transited the film and pressure

was released into air. VIS spectra were taken during rarefaction to determine if shock induced absorptions were reversible upon release of pressure. Reversal of VIS absorptions during rarefaction could be due to pressure induced band gap increases or reversible pressure induced chemistry, while irreversible changes are indicative of irreversible shock induced chemistry.[35, 37-38, 47] The VIS absorption spectra at shock pressures of 16 GPa are shown in the left frame of Fig. 4. Changes were at most 5% across the spectral range for this pressure. A strong blue slanted absorption was observed to grow during the shock at 33 GPa. This blue absorption mostly recovered during rarefaction from 33 GPa. TNT shock compressed to 40 GPa showed increased VIS absorption during the shock, which then remained constant during rarefaction. VIS spectra were also measured during the experiments conducted to obtain the high frequency MIR spectra and are shown Fig. 5. The results at 32 GPa were comparable to those at 33 GPa with similar absorption features, with similar absorptions, shape, and time scales for absorption reversal. The experiments presented at 32 GPa had a greater spread in pressure compared to those presented at 33 GPa, lowering the average VIS absorptions. TNT shock compressed to 46 GPa had qualitatively similar results to those at 40 GPa; however, the VIS absorption was approximately twice as strong. Figs. 4-7 have a red line showing the time when the shock reached the TNT/air interface, and the black line represents the time when the head of the rarefaction fan reached the TNT/aluminum drive interface, calculated using Equation 1, or Equation 4.3 from Gathers,[48] for the sound speed in a compressed material. For a given pressure (P), particle velocity (u_p), shock velocity (u_s), sound speed (c_0), and slope of the Hugoniot (shock velocity u_s vs. particle velocity u_p).[48]

$$c(P) = \frac{(c_0 + 2su_p)((c_0 + (s-1)u_p)}{c_0 + su_p} \quad (1)$$

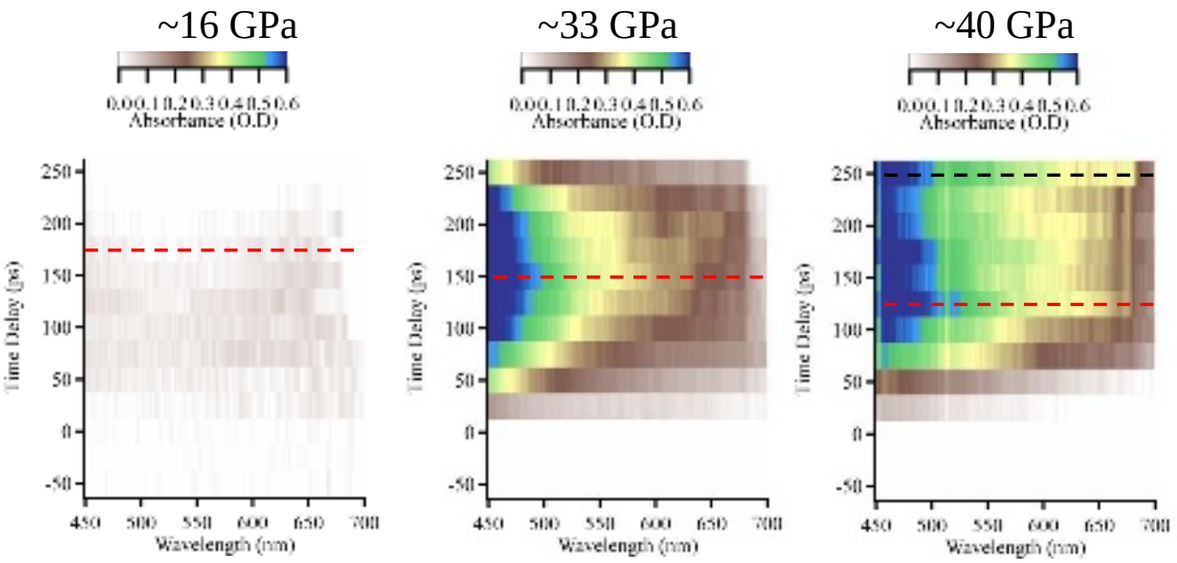

Fig. 4. Comparison of VIS absorptions for 16, 33, and 40 GPa obtained during the low frequency region MIR experiments. VIS absorptions suggested no reaction, some reaction with reversibility, and full reaction at 16, 33, and 40 GPa respectively. The feature at 520 nm at 40 GPa was an artifact present in the static spectrum.

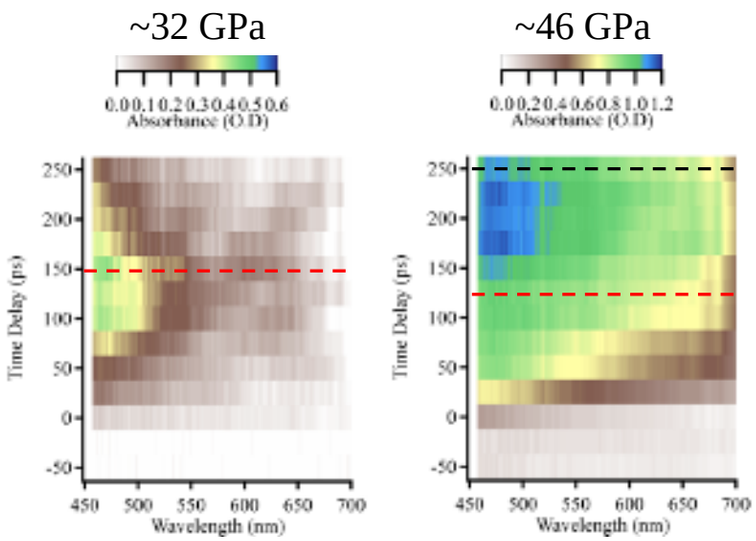

Fig. 5. Additional VIS absorption spectra obtained during the high frequency region MIR experiments. Similar results were measured for 32 GPa compared to 33 GPa with absorption growing in the shock and recovering during rarefaction. The results at 46 GPa had to be rescaled to double the optical density compared to 40 GPa. The VIS absorption measured at 46 GPa suggests more chemistry was induced than at 40 GPa.

3. *Mid-infrared (MIR) transient absorption spectroscopy*

Low frequency region MIR transmission spectra for the 16, 33, and 40 GPa cases are shown in Fig 6. Decreased spectral transmission was attributed to increased absorption in the sample. Shocked transmission is presented in Fig. 6 instead of absorption as transmission was the direct measurement performed. Absorption does not present any additional information compared to transmission. The color scale in Fig. 6 is reversed compared to the Figs. 4 and 5. In this frequency range the ν_s-NO_2 and ν_a-NO_2 at 1,350 and 1,540 cm^{-1} respectively[40] can be probed simultaneously. Multiple CH- stretches were present at 2,900-3,000 cm^{-1}, but the absorptions were very weak for these bonds compared to the NO_2 stretches.[40] The CH stretch modes were observed to decrease transmission by <5% statically at these experimental film thicknesses. A carbon dioxide (CO_2) artifact was present in this range around 2,350 cm^{-1}. Ambient CO_2 caused an artifact due to imperfect normalization of the transmission peak, which left a residual feature like that observed at 16 GPa in Fig. 6. An increasing absorption feature was observed at >2,500 cm^{-1} at 33 GPa during the shock and rarefaction. This high frequency absorption feature was not enhanced at 40 GPa, but rather MIR absorptions increased in the 1,550-2,700 cm^{-1} region. The MIR transmission background appeared to increase across the entire spectral range for the 40 GPa case.

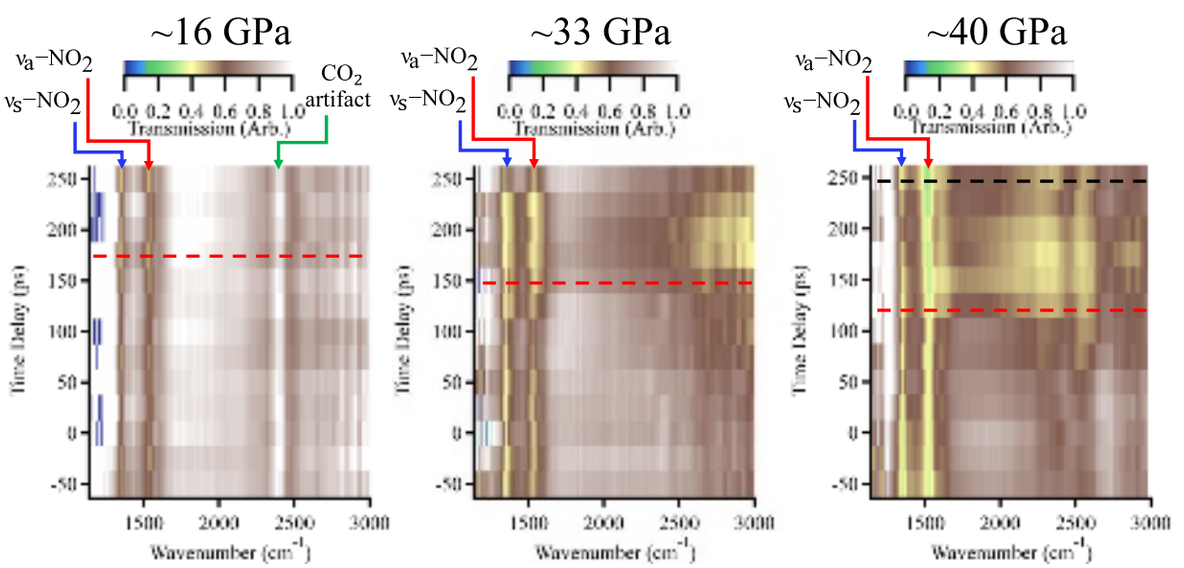

Figure 6. Comparison of the shocked transmission behavior for TNT at 16, 33, and 40 GPa. At 16 GPa no changes were observed. At 33 GPa, the NO_2 stretches broadened by ~50 cm^{-1}, and an absorption feature grew in the hydrogenic stretch region. Partial recovery was observed at 250 ps delay. At 40 GPa a broad

absorption feature was observed over most of the spectral range. There was less absorption at >2700 cm^{-1} compared to 33 GPa. The ν_a-NO_2 transmission decreased from 40% to 25%, a decrease that was not duplicated at the ν_s-NO_2 mode.

High frequency MIR spectra for shock compressed TNT at 32 and 46 GPa were also obtained, and are shown in Fig. 7. Broad absorption features >3,000 cm^{-1} appeared during the shock and did not recover upon rarefaction for both pressures. The >2,700 cm^{-1} region is where fundamental absorptions for hydrogenic stretches occur.[41] The ν_a-NO_2 absorption broadened at 32 GPa and 46 GPa, but had no significant absorption change compared to the background absorption increase.

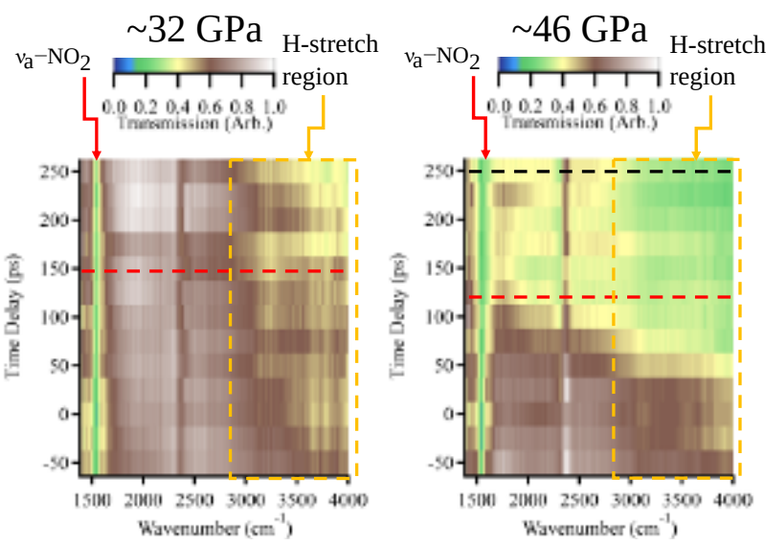

Fig. 7. Transmission spectra in the high frequency MIR region for both 32 and 46 GPa cases. At 32 GPa, the spectra showed a broad absorption feature across most of the hydrogenic stretch region with minimal absorption recovery behavior. At 46 GPa, there was a large broad absorption feature that grew during and after the passage of the shock.

IV. Discussion

1. *Shocked state from impedance matching*

Table S.1 presents all of the measured drive velocities achieved for the low, medium, and high pressure cases. All measurements of shock state were made using impedance matching. The pressures reported are most likely overestimated from the impedance matching technique.[35] The initial density used was also over-estimated as the pressures reported were crystal density, not film density. We cannot make a

suggestion on the unreactive Hugoniot deviations from impedance matching alone. Additionally, the spectroscopic methods do not provide the type of evidence to suggest if there was a volumetric changing reaction. The impedance matching technique was used in lieu of UDE for similar analysis and discussion to previous measurements on PETN.[35] All of the shock and particle velocities used in these experiments were greater than those measured by Marsh.[2] As discussed in previous publications, shock pressures in these laser shock experiments need to be larger than traditional plate impact experiments to observe reactions on the ultrafast time scales.[34, 49] We could find no Hugoniot data for the measured shock and particle velocities measured to compare to. We made a simple linear extrapolation of the unreacted TNT Hugoniot points to impedance match to, but also offer the aluminum impactor free surface measurements in the Supplemental Information.

2. VIS transient absorption spectroscopy

For the VIS absorption measurements shown in Fig. 4, at 16 GPa there was ~5% total VIS absorption changes observed. These changes can be attributed to light scattering from the drive layer surface.[37-38] When TNT was shocked to 33 GPa there was a strong, blue absorbing feature that grew during the shock; however, the transmission recovered during the rarefaction from the free surface of TNT. For 40 GPa there was an enhanced VIS absorption feature similar to that observed in the 33 GPa experiments (blue trending and broad) that did not recover upon rarefaction. Since VIS absorptions did not recover at these higher shock pressures, some irreversible change was induced in TNT. The surface roughness of the TNT films averaged out any thin film interference effects in the VIS absorptions.[35] For high pressures the blue trending absorbing feature is most likely due to absorption from intermediate species, a claim which is corroborated by the MIR absorption results. Closure of the HOMO LUMO gap is also a possible explanation of the VIS absorption measurements.[50]

For VIS transient absorptions shown in Fig. 5, at 32 GPa there was a broad blue trending VIS absorption that recovered upon release. These results were nearly identical to the 33 GPa case, except the

VIS absorptions observed were slightly weaker. At 46 GPa there were strong (>1 O.D.) absorption changes measured in the sample that did not recover upon rarefaction.

Shock induced scattering may have contributed to apparent absorption changes. Scattering measurements were performed using a photodiode off axis to the laser illumination with 1:1 image magnification of the sample in the VIS to examine this possibility. A comparison of the integrated scatter measured from shock compressed TNT and the shock aluminum drive surface is shown in Fig. 8. The free surface velocity from both samples was ~6 nm/ps, which would be >50 GPa in TNT. This free surface velocity was selected to observe the changes at a pressure that would induce reactions and the largest possible absorption changes like those in Fig 5 and 7 for 46 GPa. It was assumed that if scattering was negligible at this pressure, then it would also be negligible at lower pressures. The scattering from compressed TNT and the aluminum drive were compared to a near-perfect scattering material: polytetrafluoroethylene (PTFE). Integrated scattering (*S*) measurements were defined by equation 2,

$$S = \frac{\int_{t_1}^{t_2} V_{shock}\, dt - \int_{t_1}^{t_2} V_{preshock}\, dt}{\int_{t_1}^{t_2} V_{PTFE}\, dt} \tag{2}$$

where V is the voltage measured by the photodiode during the shock, preshock, or for PTFE tape, and t_1 and t_2 two temporal points which correspond to the temporal full-width, at half maximum to integrate the measured response for the shock, preshock, or PTFE. The preshock signal was subtracted from the shocked signal to differentiate the amount of additional scatter produced from the shockwave. The scatter from the aluminum drive surface increased linearly with time delay. Scatter decreased during the shock and rarefaction for TNT compared to the scatter measured during the preshock as shown in Fig. 8. The normalized scattering signal goes negative during the shock and rarefaction, implying the scatter is decreasing. We attribute the decrease in VIS scatter to increased VIS absorption from shock induced

chemistry. The scattering results verify the VIS absorption measurements in Fig 5 at 46 GPa was from a strongly absorbing feature, not scatter.

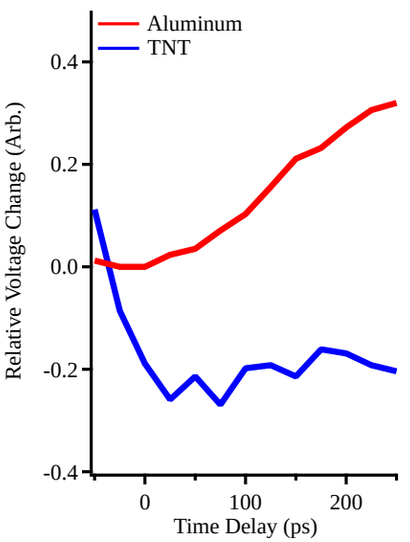

Fig. 8. Comparison of the scatter from shock compressed TNT and aluminum. Scattering from the aluminum drive layer increased during and after the shock. Scattering from TNT was negative during the shock. The shape of the scattering curve for TNT implies there may have been some scatter (increasing slope), but it is trivial compared to the absorption (negative offset).

3. MIR transient absorption spectroscopy

The low frequency MIR results at 16 GPa were similar to the VIS results; there were no significant changes observed. Broadening and shifting of the NO_2 stretches were not perceived in this pressure range. Static high pressure experiments have suggested that the ν_s-NO_2 should have shifted by 2.5 cm^{-1}/GPa, or 40 cm^{-1}.[51] The lack of frequency shifting behavior in the shocked MIR absorption experiment has been observed before and attributed to increased temperature under shock loading, although our resolution is similar to the expected frequency shift. [34-35, 42, 52]

MIR results at 33 GPa contrasted VIS results. In the VIS region, the absorptions increased during the shock and recovered during rarefaction. In the MIR region, the absorptions grew during the shock as well as during most of the rarefaction. Partial recovery of the MIR transmission spectra was observed at the

latest time delay of 250 ps. The ν_s-NO_2 and ν_a-NO_2 mode vibrations showed only broadening of ~50 cm^{-1} of the peaks, with no increased absorptions. A broad feature from 2,700-3,000 cm^{-1} increased in absorption as more material was shocked and continued increasing during rarefaction. There was some absorption on the blue side of the CO_2 stretch, but this feature was most likely an extension of the absorption feature from the hydrogenic stretch region. These MIR absorption results at 33 GPa particularly near the hydrogenic stretches suggest there was partial chemistry induced in the sample, while VIS absorptions suggest simple shock compression of the sample followed by recovery. Even in small concentrations, NH- and OH-stretches have strong absorptions.[53-56] Higher pressure experiments were performed to look for enhancement of these changes.

TNT films shocked to 40 GPa showed both the ν_s-NO_2 and ν_a-NO_2 mode vibrations broadening by 50-100 cm^{-1}. Additionally, the ν_a-NO_2 showed a slightly (37.5% compared to static) increased absorption that did not recover upon release of the pressure. An 60% absorbing feature was observed from 1,550-2,700 cm^{-1} and did not recover during rarefaction of the sample. Additionally, an absorption feature grew in the hydrogenic stretch region, but was less strong compared to either hydrogenic stretch feature present at 33 GPa or the feature that spanned the most of the MIR range (1,550-2,700 cm^{-1}) for this pressure. MIR and VIS absorptions both exhibited irreversible changes induced in TNT that were constant or grew in strength when the pressure was released.

The experimental MIR frequency region was shifted to 1,450-4,000 cm^{-1} to focus on the hydrogenic stretch region (>2800 cm^{-1}). TNT shocked to 32 GPa shows a similar hydrogenic stretch absorption feature as that observed at 33 GPa. Centered at 3,300 cm^{-1}, a broadly absorbing feature was observed to grow during the shock and for most of the rarefaction, except at the latest time delay. Again, the results for MIR absorption changes were in contrast to VIS absorption changes at this pressure. A possible explanation is that a small concentration of a strongly infrared absorbing intermediate, like an OH-stretch, is generated that does not strongly absorb in the visible spectrum.[54-57] It is possible that chemical intermediates form

which absorb only in the ultraviolet. This MIR feature was enhanced when the shock drive pressure was increased to 46 GPa. At 46 GPa, a broad strongly absorbing feature at >3,000 cm^{-1} grew during the shock and continued to grow and broaden during the rarefaction similar to the low frequency MIR range at 40 GPa. An explanation of this behavior is that some species with a strong hydrogenic stretch feature is forming, but then is further reacting, generating short lived intermediates whose infrared spectra are spectrally broad due to lifetime broadening. This result is similar to the broad product spectra observed in the shock compression of nitromethane.[52] Additionally, there are not many species or intermediates that absorb in the 1,800-2,700 cm^{-1} region for CHNO containing materials, implying that spectral broadening due to short lifetimes may be needed to explain the spectra.[58]

In summary, several of the features observed in these experiments on shock induced chemical changes in TNT are: 1.) a nearly completely reversible VIS absorption was induced at 33 GPa pressures; however, MIR absorptions did not show recovery, rather a strong absorption >2,800 cm^{-1} was observed, TNT shocked to >40 GPa showed 2.) strong, blue centered VIS absorptions with strong broadband MIR absorptions from 1,550-4,000 cm^{-1}, 3.) NO_2 stretches mostly broadened, not strongly increased or decreased in absorption, and 4.) shifting and broadening in the MIR bonds were not present at low shock pressures of 16 GPa.

Chemical mechanisms that are consistent with our results are the C-N homolysis pathway and CH_3 oxidation. Both feature OH-bond formation as one of the first critical steps in TNT shock chemistry, which agree with our results. C-H α attack and cyclization mechanisms are inconsistent with our experimental results. Diels-Alder reactions are difficult to confirm with our results at it is uncertain what infrared absorption features would be present in our observation ranges for a TNT dimer.

Conclusions

TNT films do not appear to chemically react in 175 ps when shocked to 16 GPa. TNT films exhibit large VIS absorptions when shocked to 32 or 33 GPa for 150 ps that are reversible upon rarefaction, while

broad MIR absorptions in the hydrogenic stretch region form that do not reverse upon rarefaction. TNT films shocked to 46 GPa for 125 ps exhibit very strong and very broad absorptions over thousands of wavenumbers centered in the hydrogenic stretch region and large VIS absorptions that are irreversible. These observations imply that chemistry is occurring in less than a hundred picoseconds behind the shock front in TNT shocked above 32 GPa that involves short lived strongly absorbing species such as hydrogenic bonds to oxygen or nitrogen. This result is expected for mechanisms such as C-N homolysis or methyl oxidation that form alcohol moieties.

Supplementary Material

The area analysis is shown in figures S1-S4. UDE impedance matched points are presented in tabular form in Table S1.

Data Availability Statement

Data available on request from the authors.

Acknowledgements

The authors would like to acknowledge funding for this work from ONR contract 000062867 Predictive Chemistry & Physics at Extreme Temperature and Pressure: molecules, crystals and microstructure (PCP@Xtreme). In particular, MSP thanks Prof. Steven F. Son, Purdue University, for support and encouragement. Los Alamos National Laboratory is operated by Triad National Security, LLC, for the National Nuclear Security Administration of the U.S. Department of Energy under Contract No.89233218CNA000001.

References

1. Gibbs, T.; Popolato, A. LASL Explosives. *Property Data* **1980**.
2. Marsh, S. P. *LASL shock Hugoniot data*. Univ of California Press: 1980; Vol. 5.
3. Bowden, P.; Chellappa, R.; Dattelbaum, D.; Manner, V.; Mack, N.; Liu, Z. In *The high-pressure phase stability of 2, 4, 6-trinitrotoluene (TNT)*, Journal of Physics: Conference Series, IOP Publishing: 2014; p 052006.

4. Brill, T.; James, K. Thermal decomposition of energetic materials. 62. Reconciliation of the kinetics and mechanisms of TNT on the time scale from microseconds to hours. *The Journal of Physical Chemistry* **1993,** *97* (34), 8759-8763.
5. Brill, T. B.; James, K. J. Kinetics and mechanisms of thermal decomposition of nitroaromatic explosives. *Chemical reviews* **1993,** *93* (8), 2667-2692.
6. Bulusu, S.; Axenrod, T. Electron impact fragmentation mechanisms of 2, 4, 6-trinitrotoluene derived from metastable transitions and isotopic labeling. *Organic Mass Spectrometry* **1979,** *14* (11), 585-592.
7. Dacons, J. C.; Adolph, H. G.; Kamlet, M. J. Novel observations concerning the thermal decomposition of 2, 4, 6-trinitrotoluene. *The Journal of Physical Chemistry* **1970,** *74* (16), 3035-3040.
8. Dattelbaum, D. M.; Chellappa, R. S.; Bowden, P. R.; Coe, J. D.; Margevicius, M. A. Chemical stability of molten 2, 4, 6-trinitrotoluene at high pressure. *Applied Physics Letters* **2014,** *104* (2), 021911.
9. Dodson, B.; Graham, R. In *Shock-induced organic chemistry*, AIP Conference Proceedings, American Institute of Physics: 1982; pp 42-51.
10. Dubikhin, V.; Matveev, V.; Nazin, G. Thermal decomposition of 2, 4, 6-trinitrotoluene in melt and solutions. *Russian chemical bulletin* **1995,** *44* (2), 258-263.
11. Guidry, R. M.; Davis, L. P. Thermochemical decomposition of explosives. I. TNT kinetic parameters determined from ESR investigations. *Thermochimica Acta* **1979,** *32* (1-2), 1-18.
12. Jenkins, T. F.; Murrmann, R. P.; Leggett, D. C. Mass spectra of isomers of trinitrotoluene. *Journal of Chemical and Engineering Data* **1973,** *18* (4), 438-439.
13. Makashir, P.; Kurian, E. Spectroscopic and thermal studies on 2, 4, 6-trinitro toluene (TNT). *Journal of thermal analysis and calorimetry* **1999,** *55* (1), 173-185.
14. Monat, J.; Gump, J. In *Decomposition products of RDX and TNT after resonant laser excitation*, AIP Conference Proceedings, American Institute of Physics: 2009; pp 1309-1312.
15. Robert Carper, W.; Cameron Dorey, R.; Tomer, K. B.; Crow, F. W. Mass spectral fragmentation pathways in 2, 4, 6-trinitrotoluene derived from a MS/MS unimolecular and collisionally activated dissociation study. *Organic mass spectrometry* **1984,** *19* (12), 623-626.
16. Rogers, R. N. Combined pyrolysis and thin-layer chromatography. Study of decomposition mechanisms. *Analytical Chemistry* **1967,** *39* (7), 730-733.
17. Shackelford, S.; Beckmann, J.; Wilkes, J. Deuterium isotope effects in the thermochemical decomposition of liquid 2, 4, 6-trinitrotoluene: application to mechanistic studies using isothermal differential scanning calorimetry analysis. *The Journal of Organic Chemistry* **1977,** *42* (26), 4201-4206.
18. Swanson, J. T.; Davis, L. P.; Dorey, R. C.; Carper, W. R. An EPR study of the thermal decomposition of molten 2, 4, 6-trinitrotoluene and its isotopic analogs. *Magnetic Resonance in Chemistry* **1986,** *24* (9), 762-767.
19. Yinon, J. Mass spectral fragmentation pathways in 2, 4, 6-trinitroaromatic compounds. A tandem mass spectrometric collision induced dissociation study. *Organic mass spectrometry* **1987,** *22* (8), 501-505.
20. Zitrin, S.; Yinon, J. Chemical ionization mass spectra of 2, 4, 6-trinitroaromatic compounds. *Organic Mass Spectrometry* **1976,** *11* (4), 388-393.
21. Murray, J. S.; Lane, P.; Politzer, P.; Bolduc, P. R. A relationship between impact sensitivity and the electrostatic potentials at the midpoints of C · NO2 bonds in nitroaromatics. *Chemical physics letters* **1990,** *168* (2), 135-139.

22. Cohen, R.; Zeiri, Y.; Wurzberg, E.; Kosloff, R. Mechanism of thermal unimolecular decomposition of TNT (2, 4, 6-trinitrotoluene): a DFT study. *The Journal of Physical Chemistry A* **2007,** *111* (43), 11074-11083.
23. Engelke, R.; Blais, N. C.; Sheffield, S. A.; Sander, R. K. Production of a chemically-bound dimer of 2, 4, 6-TNT by transient high pressure. *The Journal of Physical Chemistry A* **2001,** *105* (28), 6955-6964.
24. Kamlet, M.; Adolph, H. The relationship of impact sensitivity with structure of organic high explosives. II. Polynitroaromatic explosives. *Propellants, Explosives, Pyrotechnics* **1979,** *4* (2), 30-34.
25. Liu, H.; He, Y.; Li, J.; Zhou, Z.; Ma, Z.; Liu, S.; Dong, X. ReaxFF molecular dynamics simulations of shock induced reaction initiation in TNT. *AIP Advances* **2019,** *9* (1), 015202.
26. Owens, F. Relationship between impact induced reactivity of trinitroaromatic molecules and their molecular structure. *Journal of Molecular Structure: THEOCHEM* **1985,** *121*, 213-220.
27. Owens, F. Calculation of energy barriers for bond rupture in some energetic molecules. *Journal of Molecular Structure: THEOCHEM* **1996,** *370* (1), 11-16.
28. Owens, F.; Sharma, J. X-ray photoelectron spectroscopy and paramagnetic resonance evidence for shock-induced intramolecular bond breaking in some energetic solids. *Journal of Applied Physics* **1980,** *51* (3), 1494-1497.
29. Owens, F. J.; Jayasuriya, K.; Abrahmsen, L.; Politzer, P. Computational analysis of some properties associated with the nitro groups in polynitroaromatic molecules. *Chemical physics letters* **1985,** *116* (5), 434-438.
30. Quenneville, J.; Germann, T. C. A quantum chemistry study of Diels–Alder dimerizations in benzene and anthracene. *The Journal of chemical physics* **2009,** *131* (2), 024313.
31. Rice, B. M.; Sahu, S.; Owens, F. J. Density functional calculations of bond dissociation energies for NO2 scission in some nitroaromatic molecules. *Journal of Molecular Structure: THEOCHEM* **2002,** *583* (1-3), 69-72.
32. Fowles, G.; Duvall, G.; Asay, J.; Bellamy, P.; Feistmann, F.; Grady, D.; Michaels, T.; Mitchell, R. Gas gun for impact studies. *Review of Scientific Instruments* **1970,** *41* (7), 984-996.
33. Rom, N.; Hirshberg, B.; Zeiri, Y.; Furman, D.; Zybin, S. V.; Goddard III, W. A.; Kosloff, R. First-principles-based reaction kinetics for decomposition of hot, dense liquid TNT from ReaxFF multiscale reactive dynamics simulations. *The Journal of Physical Chemistry C* **2013,** *117* (41), 21043-21054.
34. Powell, M. S.; Bowlan, P. R.; Son, S. F.; Bolme, C. A.; Brown, K. E.; Moore, D. S.; McGrane, S. D. A benchtop shock physics laboratory: Ultrafast laser driven shock spectroscopy and interferometry methods. *Review of Scientific Instruments* **2019,** *90* (6), 063001.
35. Powell, M. S.; Sakano, M. N.; Cawkwell, M. J.; Bowlan, P. R.; Brown, K. E.; Bolme, C. A.; Moore, D. S.; Son, S. F.; Strachan, A.; McGrane, S. D. Insight into the Chemistry of PETN Under Shock Compression Through Ultrafast Broadband Mid-Infrared Absorption Spectroscopy. *The Journal of Physical Chemistry A* **2020,** *124*, 7031-7046.
36. Bolme, C. A. Ultrafast dynamic ellipsometry of laser driven shock waves. Massachusetts Institute of Technology, MIT, 2008.
37. Brown, K. E.; McGrane, S. D.; Bolme, C. A.; Moore, D. S. Ultrafast Chemical Reactions in Shocked Nitromethane Probed with Dynamic Ellipsometry and Transient Absorption Spectroscopy. *Journal of Physical Chemistry A* **2014,** *118* (14), 2559-2567.

38. Dang, N. C.; Bolme, C. A.; Moore, D. S.; McGrane, S. D. Shock Induced Chemistry In Liquids Studied With Ultrafast Dynamic Ellipsometry And Visible Transient Absorption Spectroscopy. *Journal of Physical Chemistry A* **2012,** *116* (42), 10301-10309.
39. Whitley, V. H.; McGrane, S. D.; Eakins, D. E.; Bolme, C. A.; Moore, D. S.; Bingert, J. F. The elastic-plastic response of aluminum films to ultrafast laser-generated shocks. *Journal of Applied Physics* **2011,** *109* (1), 1-4.
40. Nash, C.; Nelson, T.; Stewart, J.; Carper, W. *Molecular structure and vibrational analysis of 2, 4, 6-trinitrotoluene and 2, 4, 6-trinitrotoluene-a-d3*; FRANK J SEILER RESEARCH LAB UNITED STATES AIR FORCE ACADEMY CO: 1989.
41. Coates, J. Interpretation of infrared spectra, a practical approach. In *Encyclopedia of analytical chemistry: applications, theory and instrumentation*, Meyers, R. A., Ed. John Wiley and Sons: 2006.
42. Powell, M.; Bowlan, P.; Son, S.; McGrane, S. Ultrafast Mid-Infrared Spectroscopy on Shocked Thin Film Explosive Crystals. In *16th International Detonation Symposium*, Office of Naval Research: Cambridge, MD, 2018; pp 790-796.
43. Fondren, N. S.; Fondren, Z. T.; Unruh, D. K.; Weeks, B. L. Effects of Solution Conditions on Polymorph Development in 2, 4, 6-Trinitrotoluene. *Crystal Growth & Design* **2019,** *20* (2), 568-579.
44. Gallagher, H. G.; Sherwood, J. N. Polymorphism, twinning and morphology of crystals of 2, 4, 6-trinitrotoluene grown from solution. *Journal of the Chemical Society, Faraday Transactions* **1996,** *92* (12), 2107-2116.
45. Miller, G.; Garroway, A. *A review of the crystal structures of common explosives. Part I: RDX, HMX, TNT, PETN, and tetryl*; NAVAL RESEARCH LAB WASHINGTON DC: 2001.
46. Vrcelj, R. M.; Gallagher, H. G.; Sherwood, J. N. Polymorphism in 2, 4, 6-trinitrotoluene crystallized from solution. *Journal of the American Chemical Society* **2001,** *123* (10), 2291-2295.
47. Brown, K. E.; Bolme, C. A.; McGrane, S. D.; Moore, D. S. Ultrafast shock-induced chemistry in carbon disulfide probed with dynamic ellipsometry and transient absorption spectroscopy. *Journal of Applied Physics* **2015,** *117* (8), 085903.
48. Gathers, G. R. Selected topics in shock wave physics and equation of state modeling. World Scientific: 1994; p 270.
49. McGrane, S. D.; Brown, K. E.; Bolme, C. A.; Moore, D. S. Interaction between measurement time and observed Hugoniot cusp due to chemical reactions. *AIP Conference Proceedings* **2017,** *1793* (1), 030033.
50. Kuklja, M. M.; Stefanovich, E. V.; Kunz, A. B. An excitonic mechanism of detonation initiation in explosives. *The Journal of Chemical Physics* **2000,** *112* (7), 3417-3423.
51. Goryainova, S. V.; Volodinb, V. A.; Danilenkod, A. M. Raman spectroscopic study of 2, 4, 6–trinitrotoluene at high pressure. *Physics Express* **2011,** *1* (4), 242-246.
52. Bowlan, P.; Powell, M.; Perriot, R.; Martinez, E.; Kober, E. M.; Cawkwell, M. J.; McGrane, S. Probing ultrafast shock-induced chemistry in liquids using broad-band mid-infrared absorption spectroscopy. *The Journal of chemical physics* **2019,** *150* (20), 204503.
53. Bernstein, H. The average XH stretching frequency as a measure of XH bond properties. *Spectrochimica Acta* **1962,** *18* (2), 161-170.
54. Brown, T. L. Infrared intensities and molecular structure. *Chemical Reviews* **1958,** *58* (3), 581-608.
55. Kjaergaard, H. G.; Daub, C. D.; Henry, B. R. The role of electron correlation on calculated XH-stretching vibrational band intensities. *Molecular Physics* **1997,** *90* (2), 201-213.

56. Rao, C.; Venkataraghavan, R. Correlations of Infrared Group Frequencies and Band Intensities in Organic Molecules with Substituent Constants: A Statistical Evaluation. *Canadian Journal of Chemistry* **1961,** *39* (9), 1757-1764.
57. Silverstein, R. M.; Bassler, G. C.; Morrill, T. C. Spectrometric identification of organic compounds. *Journal of Chemical Education* **1981,** *39* (11), 546-553.
58. Pierson, R. H.; Fletcher, A. N.; Gantz, E. S. C. Catalog of infrared spectra for qualitative analysis of gases. *Analytical Chemistry* **1956,** *28* (8), 1218-1239.

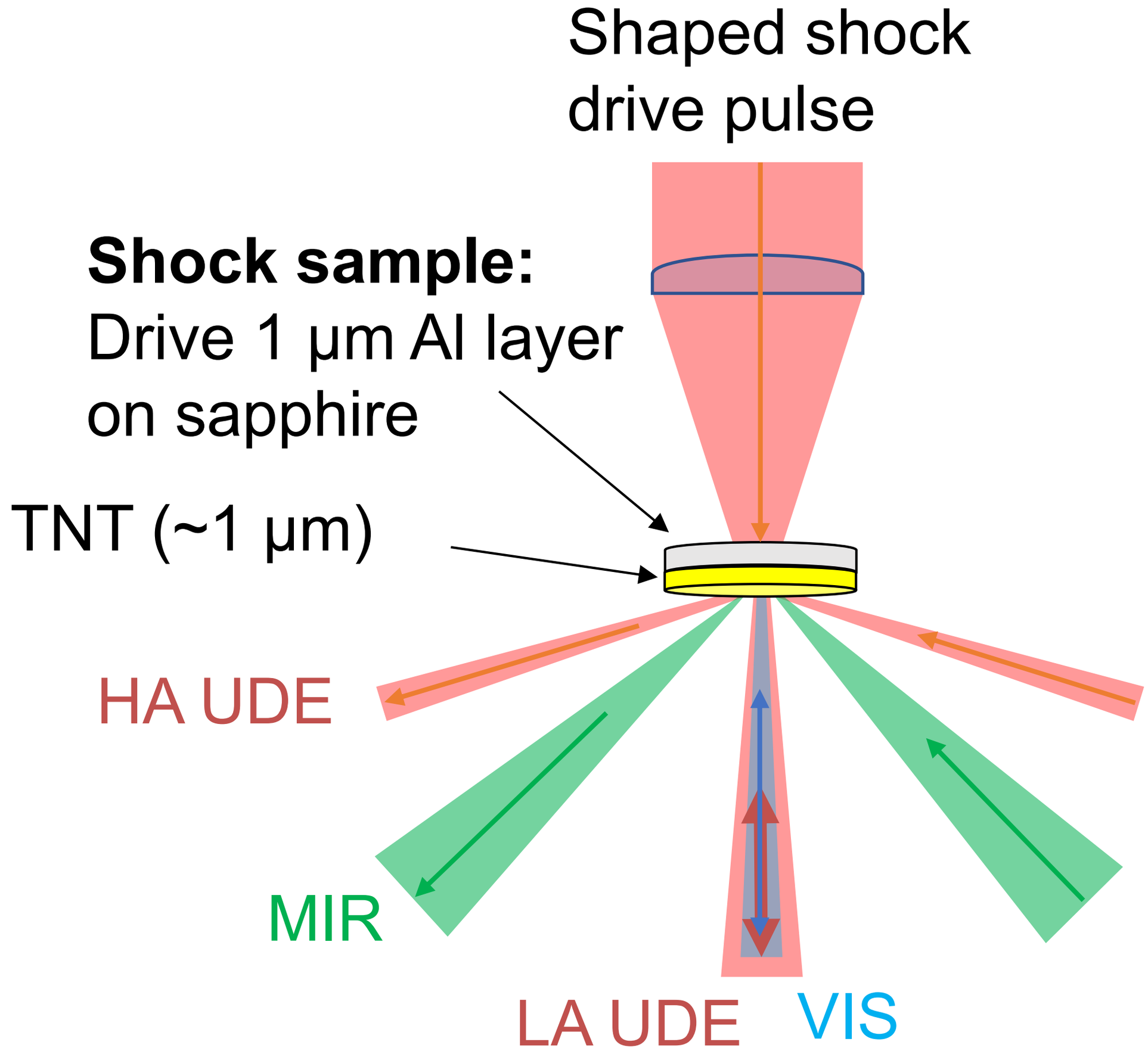
Shaped shock drive pulse
Shock sample:
Drive 1 μm Al layer on sapphire
TNT (~1 μm)
HA UDE
MIR
LA UDE
VIS

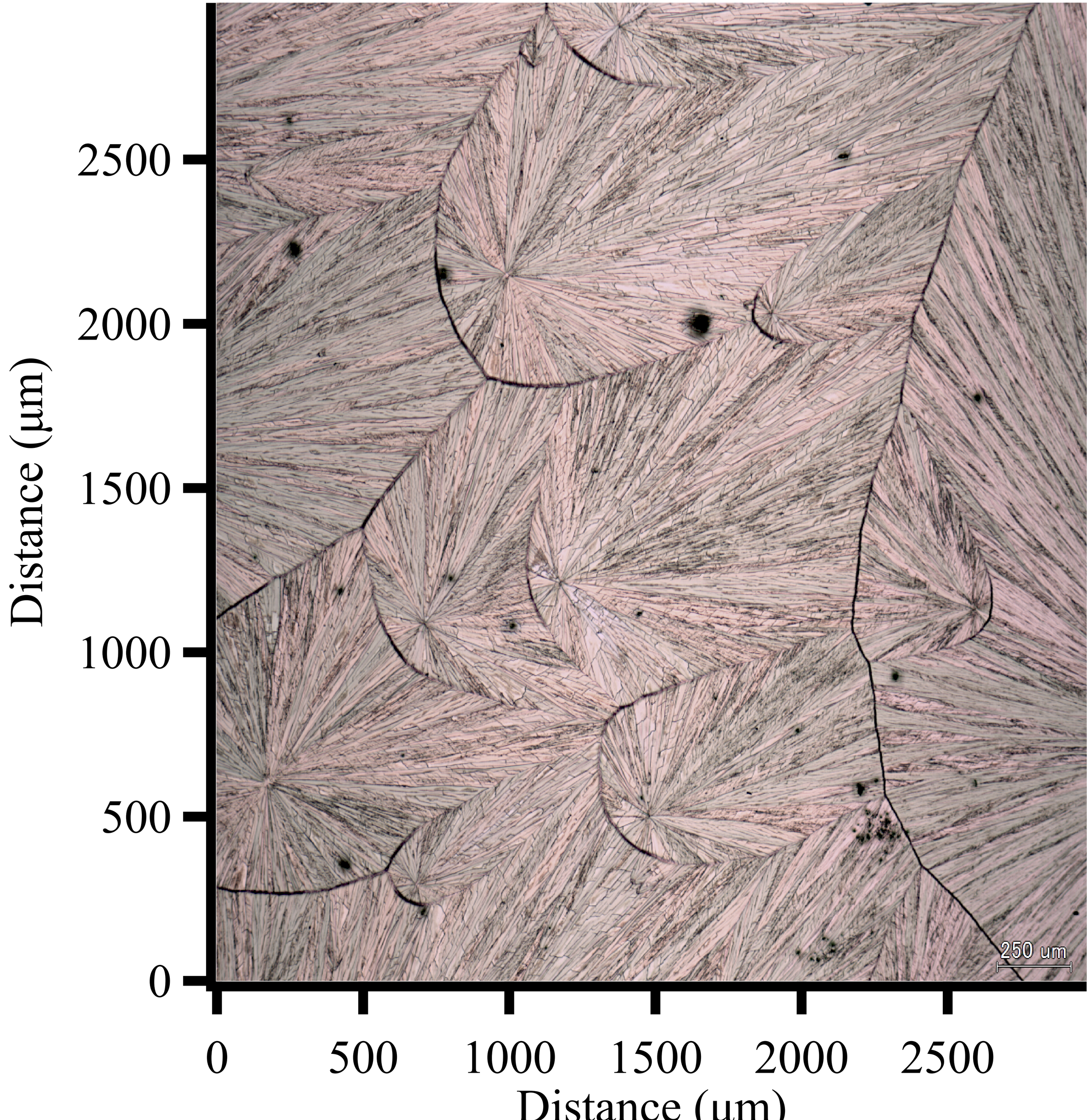
2500
2000
1500
1000
500
0
Distance (µm)
250 um
0
500
1000
1500
2000
2500
Distance (µm)

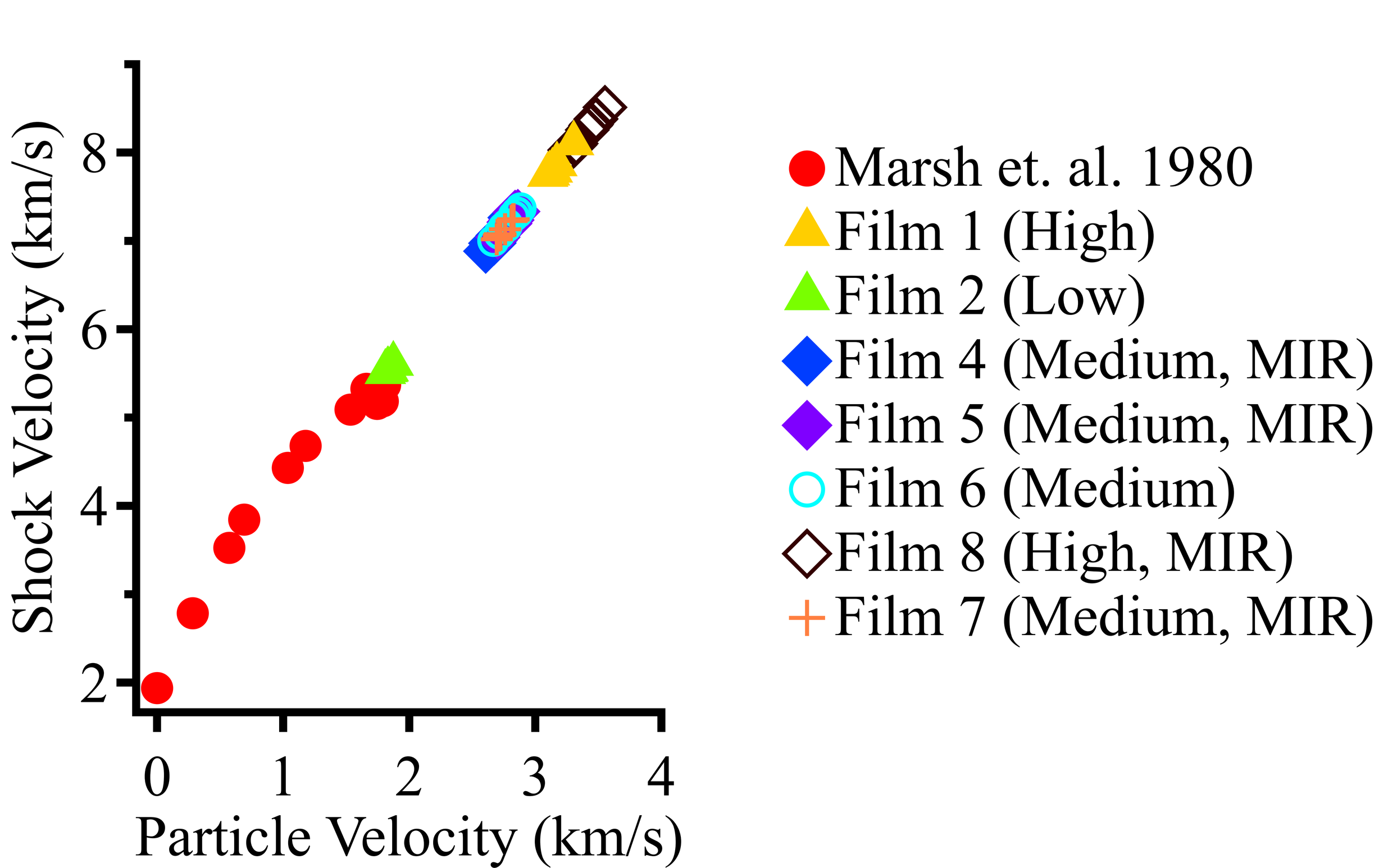
Shock Velocity (km/s)
2
4
6
8
0
1
2
3
4
Particle Velocity (km/s)
Marsh et. al. 1980
Film 1 (High)
Film 2 (Low)
Film 4 (Medium, MIR)
Film 5 (Medium, MIR)
Film 6 (Medium)
Film 8 (High, MIR)
Film 7 (Medium, MIR)

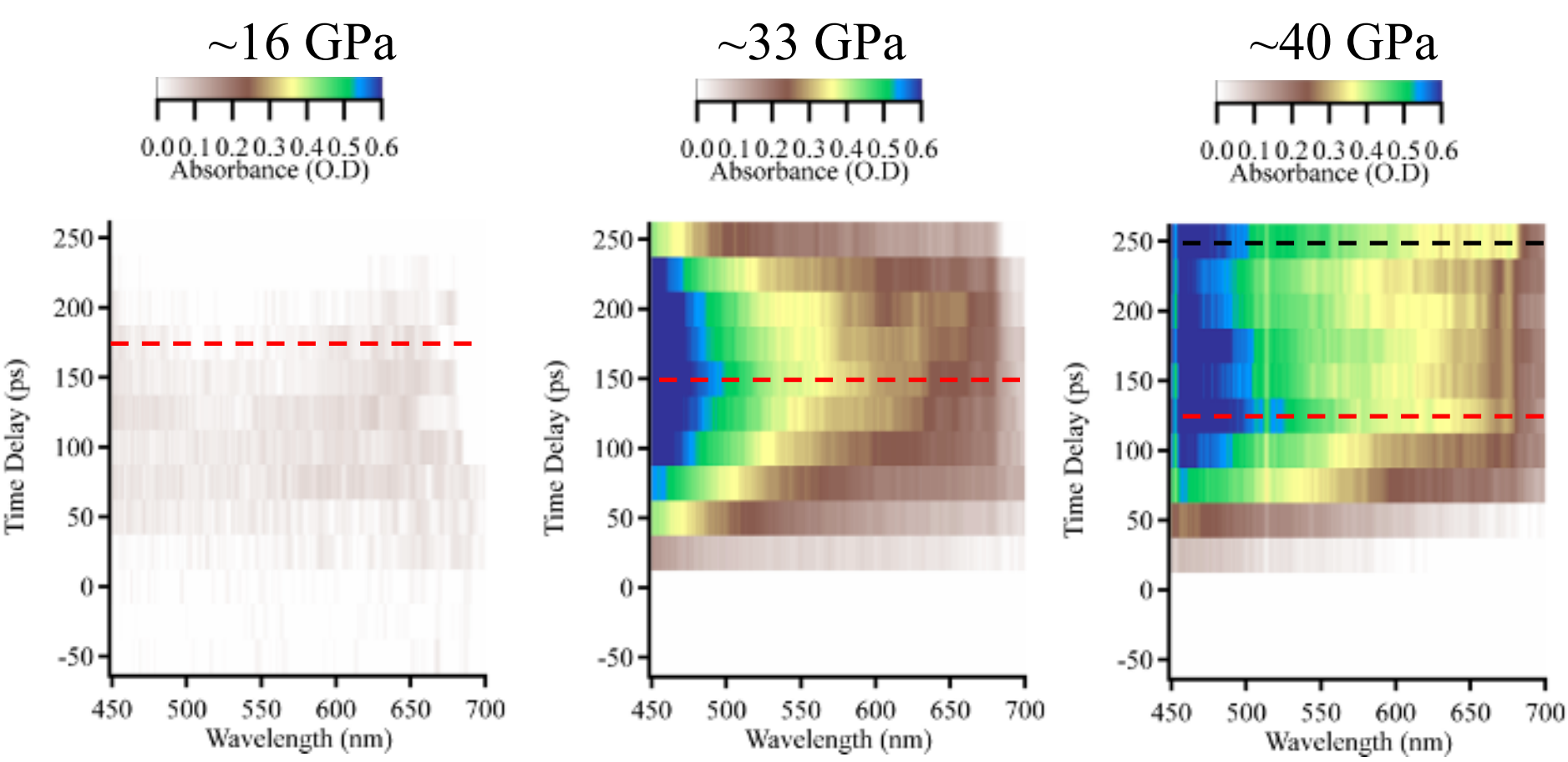
~16 GPa
~33 GPa
~40 GPa
0.0 0.1 0.2 0.3 0.4 0.5 0.6
Absorbance (O.D)
Time Delay (ps)
250
200
150
100
50
0
-50
450 500 550 600 650 700
Wavelength (nm)

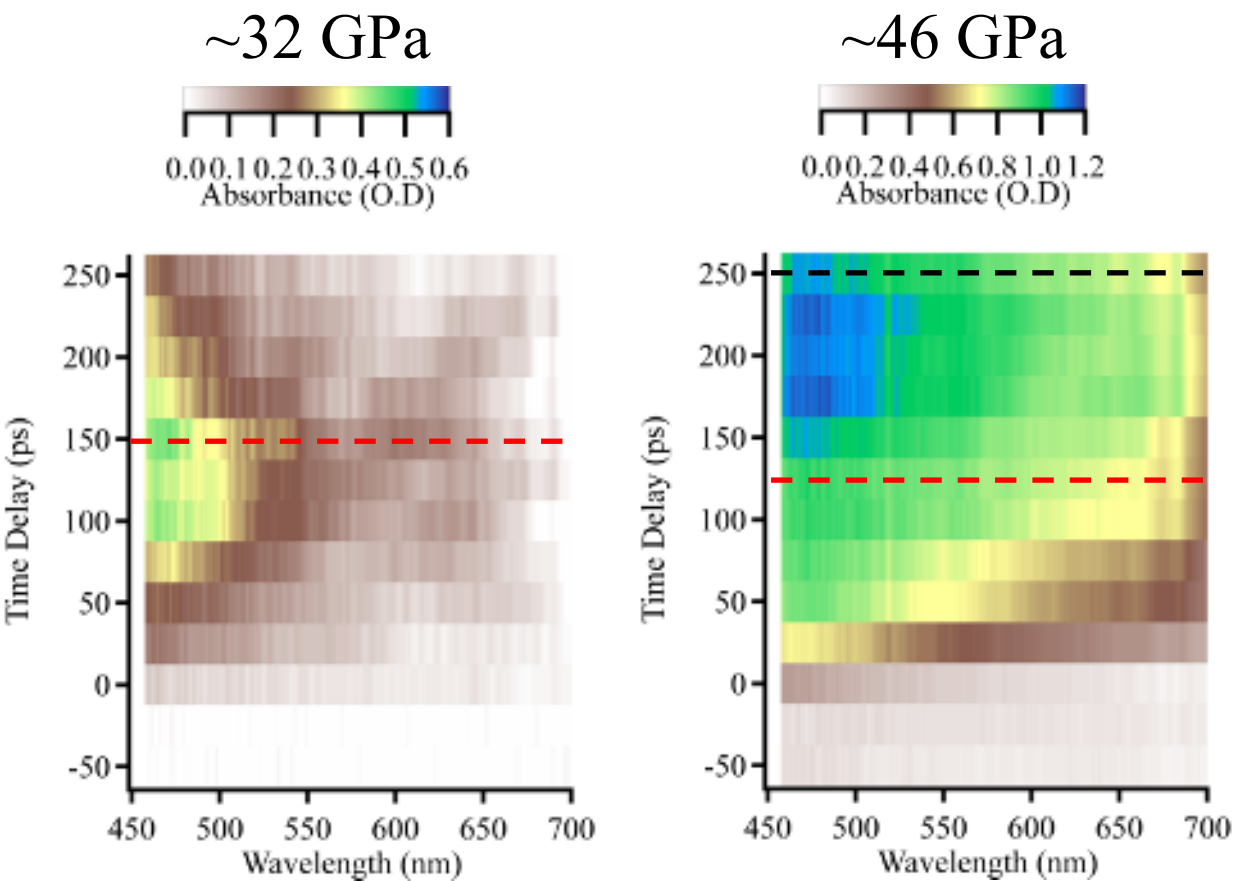
~32 GPa
0.0 0.1 0.2 0.3 0.4 0.5 0.6
Absorbance (O.D)
Time Delay (ps)
250
200
150
100
50
0
-50
450 500 550 600 650 700
Wavelength (nm)
~46 GPa
0.0 0.2 0.4 0.6 0.8 1.0 1.2
Absorbance (O.D)
Time Delay (ps)
250
200
150
100
50
0
-50
450 500 550 600 650 700
Wavelength (nm)

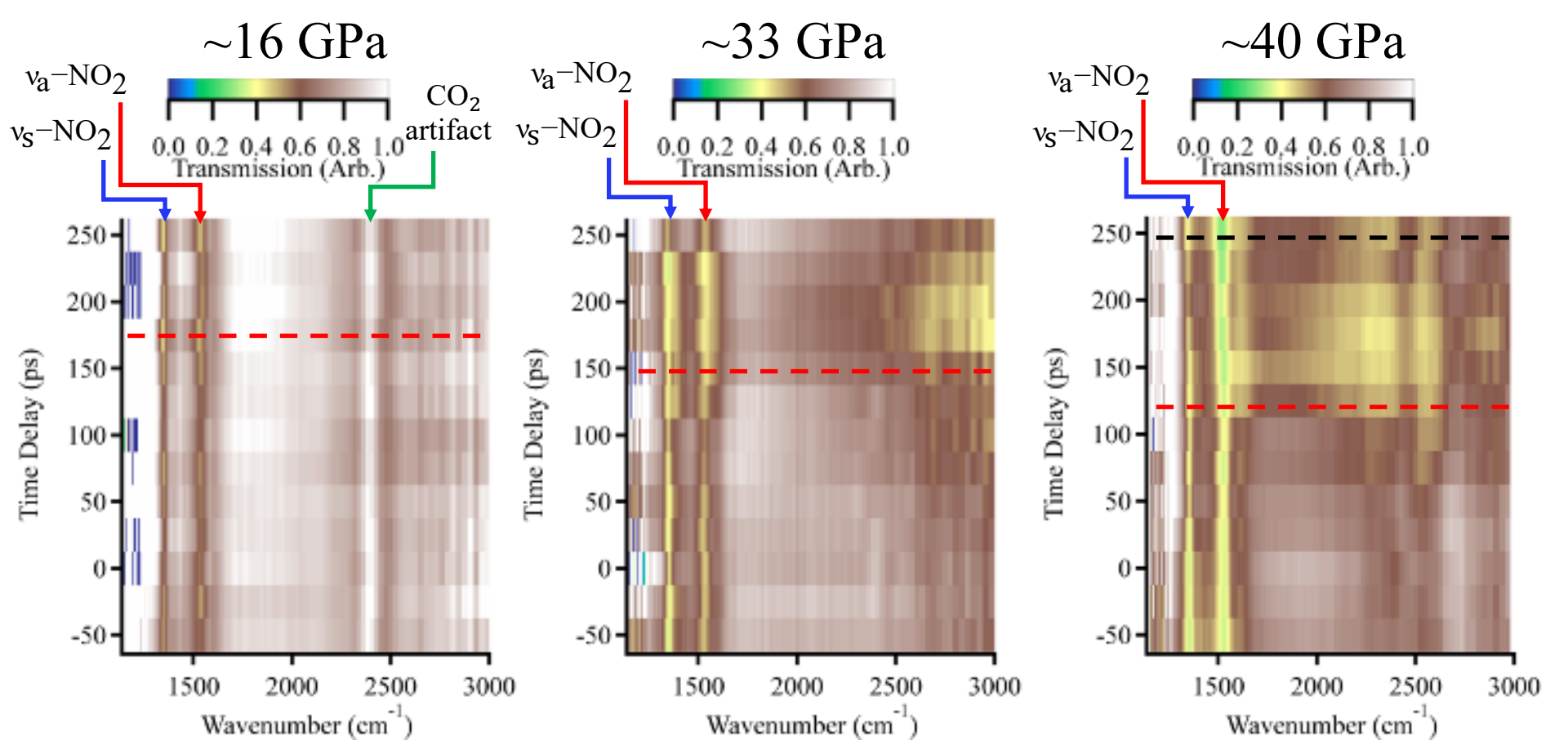
~16 GPa
~33 GPa
~40 GPa
ν_a–NO_2
ν_s–NO_2
CO_2 artifact
0.0 0.2 0.4 0.6 0.8 1.0
Transmission (Arb.)
Time Delay (ps)
250
200
150
100
50
0
-50
1500
2000
2500
3000
Wavenumber (cm^{-1})

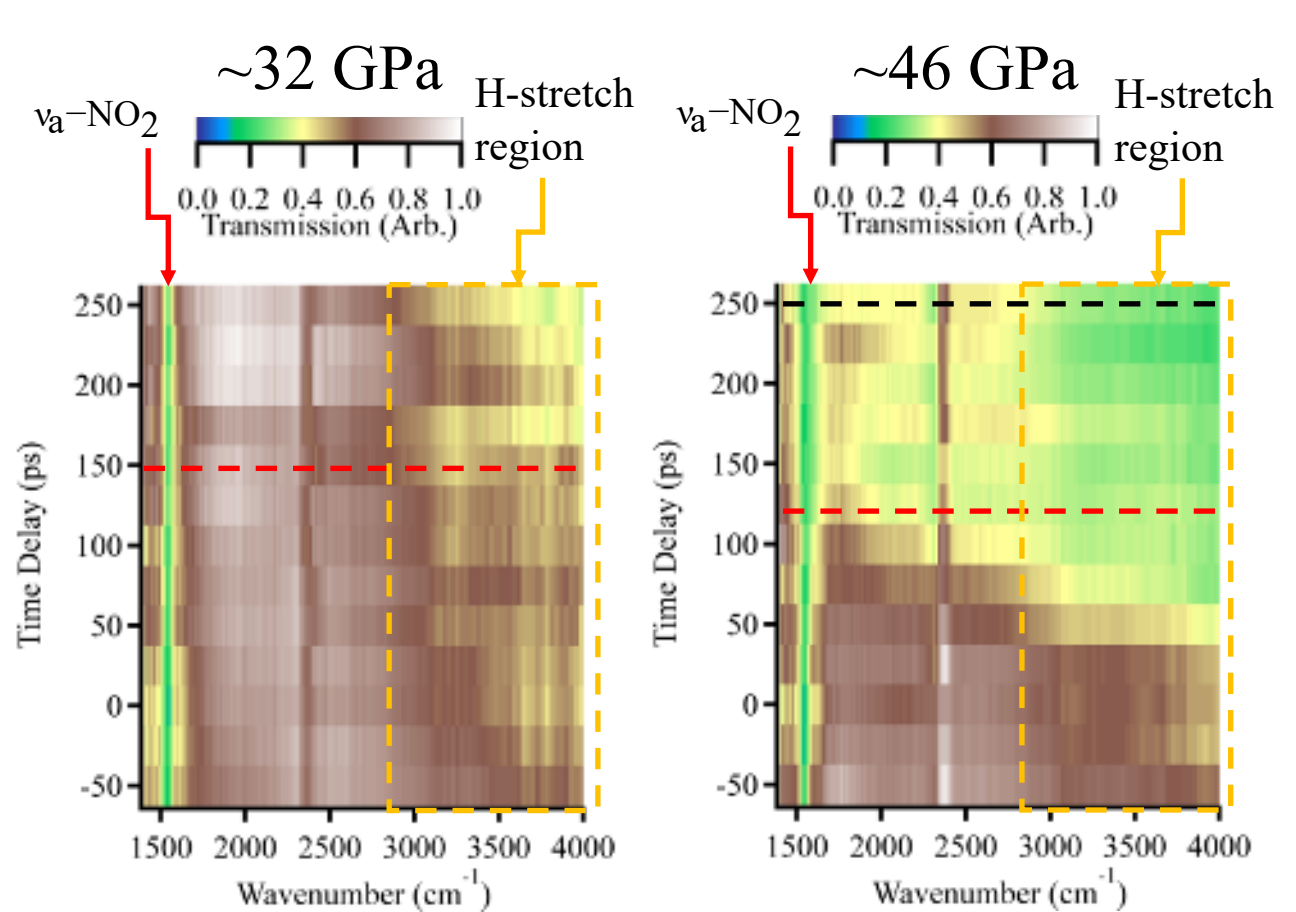
~32 GPa
ν_a–NO_2
H-stretch region
0.0 0.2 0.4 0.6 0.8 1.0
Transmission (Arb.)
Time Delay (ps)
250
200
150
100
50
0
-50
1500 2000 2500 3000 3500 4000
Wavenumber (cm^{-1})
~46 GPa
ν_a–NO_2
H-stretch region
0.0 0.2 0.4 0.6 0.8 1.0
Transmission (Arb.)
Time Delay (ps)
250
200
150
100
50
0
-50
1500 2000 2500 3000 3500 4000
Wavenumber (cm^{-1})

Aluminum
TNT
0.4
0.2
0.0
-0.2
-0.4
Relative Voltage Change (Arb.)
0
100
200
Time Delay (ps)